Spectrochimica Acta Part A: Molecular and Biomolecular Spectroscopy 114 (2013) 509–519

Contents lists available at SciVerse ScienceDirect

Spectrochimica Acta Part A: Molecular and Biomolecular Spectroscopy

journal homepage: www.elsevier.com/locate/saa

Experimental and theoretical FTIR and FT-Raman spectroscopic analysis of 1-pyrenecarboxylic acid

M. Karabacak [a], M. Cinar [b], M. Kurt [c], P. Chinna babu [d], N. Sundaraganesan [d,*]

[a] Department of Mechatronics Engineering, HFT Technology Faculty, Celal Bayar University, 45400 Turgutlu, Manisa, Turkey
[b] Department of Science Education, Bayburt University, 69000 Bayburt, Turkey
[c] Department of Physics, Ahi Evran University, 40100 Kirsehir, Turkey
[d] Department of Physics (Engg.), Annamalai University, Annamalai Nagar, 608 002 Chidambaram, Tamil Nadu, India

HIGHLIGHTS

- The FTIR and FT-Raman spectra of 1-pyrenecarboxylic acid were recorded.
- The vibrational frequencies were calculated by DFT method and compared.
- NMR, NLO and MEP analysis were also carried out.
- UV–Vis spectra were recorded and compared with calculated ones.

GRAPHICAL ABSTRACT

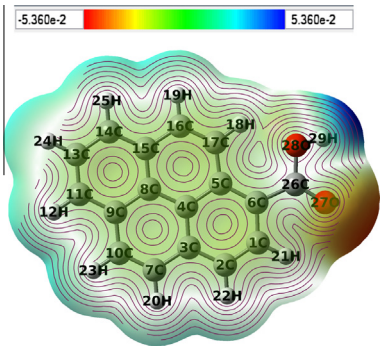

ARTICLE INFO

Article history:
Received 1 March 2013
Received in revised form 15 May 2013
Accepted 24 May 2013
Available online 4 June 2013

Keywords:
DFT
Vibrational spectra
NMR
NLO
Electronic properties
1-Pyrenecarboxylic acid

ABSTRACT

The title molecule 1-pyrenecarboxylic acid (1PCA) has been characterized by FTIR, FT-Raman, NMR and UV–Vis spectral analyses. The molecular geometry, harmonic vibrational modes, the corresponding wavenumbers and IR intensities of 1PCA were calculated by DFT method with 6-311G(d,p) basis set. The assignments of the fundamentals were proposed on the basis of total energy distribution (TED) calculations. The calculated ^{13}C and ^{1}H NMR chemical shifts using gauge including atomic orbitals (GIAOs) approach are in good agreement with the observed chemical shifts. The polarizability and first order hyperpolarizability of the title molecule were calculated and interpreted. Using TD-DFT method, the electronic transitions have been compared with the experimental wavelengths. The molecular electrostatic potential map was used for prediction of possible hydrogen and oxygen bonding sites 1PCA molecule.

Introduction

A wide variety of industrially and biologically relevant molecules feature the carboxyl group or a close relation thereof, making the study of its interaction with surfaces of considerable relevance [1,2]. Compounds having a carboxyl group are widely distributed in nature and play important roles at trace levels in the regulation of a variety of physiological and biological functions. Therefore, the characterization and determination of carboxylic acids in biological fluids and tissues are often of clinical value, especially in the elucidation of the nature, diagnosis and treatment of a number of metabolic and nutrition disorders [3]. Pyrene is an aromatic hydrocarbon having unique photophysical characteristics, which include a relatively long lifetime of its singlet excited

* Corresponding author. Tel.: +91 9442068405.
E-mail address: sundaraganesan_n@yahoo.com (N. Sundaraganesan).

1386-1425/$ - see front matter © 2013 Elsevier B.V. All rights reserved.
http://dx.doi.org/10.1016/j.saa.2013.05.086

state and a high quantum yield of fluroscence [4]. Pyrene and its derivatives have often been used as sensitizers to initiate electron transfer reactions [5,6].

Literature survey reveals that to the best of our knowledge, the results based on quantum chemical calculations, vibrational spectral studies and HOMO–LUMO and MEP analyses on 1PCA molecule have no reports. Hence, we desired to investigate a spectroscopic characterization of 1PCA molecule with a view to get some insight into structure–function relationship through spectra-structure correlation. In order to achieve this objective, FT-IR, NMR and UV–Vis spectroscopic studies along with HOMO (highest occupied molecular orbital)-LUMO (lowest occupied molecular orbital) and MEP analysis have been performed by applying density functional theory calculations based on B3LYP/6-311G(d,p) level.

The quantum chemical calculations have been proven to be an important tool for the investigations of relationships between structures and spectral properties of the organic molecules and for the interpretation of experimental data arising from industrial interest and applications. By means of increasing development of computational chemistry in the past decade, the research of theoretical modeling of drug design, functional material design, etc., has become much more established than ever.

Experimental details

The 1-pyrenecarboxylic acid sample was purchased from Sigma–Aldrich Company with a stated purity 97% and it was used as such without further purification. The sample was prepared using a KBr disk technique because of solid state. The FTIR spectrum of 1PCA molecule was recorded in the region 4000–400 cm^{-1} on a Perkin Elmer FTIR spectrometer calibrated using polystyrene bands. The FT-Raman spectrum of the sample was recorded using 1064 nm line of Nd:YAG laser excitation wavelength in the region 50–4000 cm^{-1}on a Bruker RFS 100/S FT-Raman spectrometer. The detector is a liquid nitrogen cooled Ge detector. Five hundred scans were accumulated at 4 cm^{-1} resolution using a laser power of 100 mW. The experimental FT-IR and FT-Raman spectra along with the theoretically simulated IR and Raman spectra using DFT/B3LYP/6-31G(d,p) level of calculations are shown in Figs. 1 and 2. The proton spectra at 300 MHz were recorded at room temperature on a AV 300 NMR spectrometer. The samples were prepared by dissolving about 0.5 g of the sample in 2.5 ml of DMSO containing 1%. The TMS Proton spectrum has the following experimental parameters: number of scans 16: spectral width 6172.84 Hz; acquisition time 2.65 s. The carbon (^{13}C) NMR spectra at 300 MHz were recorded at room temperature on the same instrument. The samples were prepared by dissolving about 10 mg of the sample in 0.5 ml of DMSO 1%. The carbon spectrum has the following experimental parameters: number of scans 127; spectral width 17985.61 Hz; acquisition time 1.82 s.

Computational details

All the calculations in the present work were executed with the Gaussian 03 program [7]. In the DFT calculations, the B3LYP functional combined with 6-311G(d,p) basis set were used for geome-

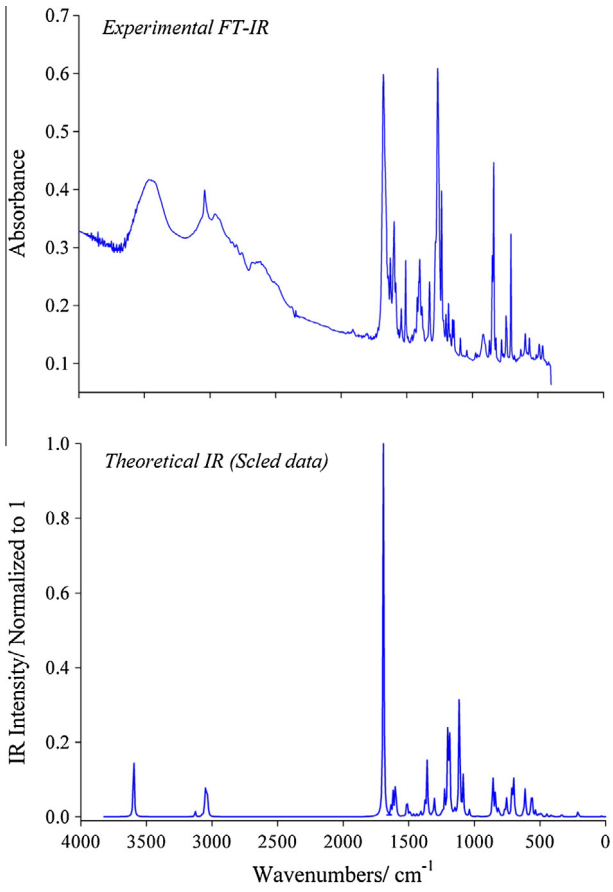

Fig. 1. Comparison of experimental and theoretical (B3LYP/6-311G(d,p)) FT-IR spectra for 1PCA.

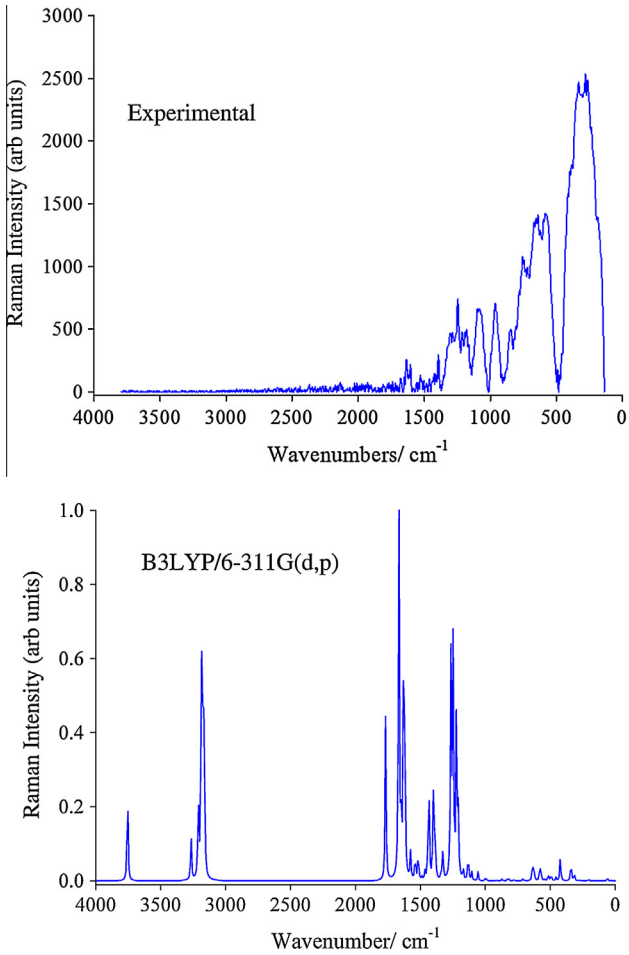

Fig. 2. Comparison of experimental and theoretical (B3LYP/6-311G (d,p)) FT-Raman spectra for 1PCA.

try optimization, computation of harmonic vibrational frequencies, calculation of α, β components and excitation energies. The B3LYP functional is most popular density functional method and can provide reliable predictions on the structures and vibrational frequencies [8,9]. All vibrational mode frequencies were found to be real which indicates that a true minimum on hypersurface of total energy was found. By using Gauss-View molecular visualization program [10], the vibrational bands assignments have been made. The vibrational assignments of the normal modes were made on the basis of the TED calculated by using VEDA 4 program [11]. The electronic absorption spectra were calculated using the time-dependent density functional theory (TD-DFT) method [12–15]. Also, it is calculated in gas phase, methanol, DMSO and water using the Polarizable Continuum Model (PCM) [16–19]. To investigate the reactive sites of the compound the molecular electrostatic potential was evaluated using the DFT method. The linear polarizability and first hyperpolarizability properties of the compound were obtained from molecular polarizabilities based on theoretical calculations.

Prediction of Raman intensities

The Raman activities (S_i) calculated with Gaussian 03 program [7] converted to relative Raman intensities (I_{Ra}) using the following relationship derived from the intensity theory of Raman scattering [20,21],

$$I_i = \frac{f(v_0 - v_i)^4 S_i}{v_i[1 - \exp(-hcv_i/kT)]}$$

where v_0 is the laser exciting wavenumber in cm^{-1} (in this work, we have used the excitation wavenumber v_0 = 9398.5 cm^{-1}, which corresponds to the wavelength of 1064 nm of Nd:YAG laser), v_i is the vibrational wavenumber of *i*th normal mode (cm^{-1}), while S_i is the Raman scattering activity of the normal mode v_i. f (is a constant equal to 10^{-12}) is a suitably chosen common factor for all peak intensities. *h, k, c* and *T* are Planck and Boltzmann constants, speed of light and temperature in Kelvin, respectively. For simulation, the calculated FT-Raman spectra have been plotted using pure Lorentizian band shape with a band width of Full Width at Half Maximum (FWHM) of 10 cm^{-1}.

Results and discussion

Molecular geometry

The geometry of the molecule under investigation is considered by possessing C_S point group symmetry. The optimized molecular structures obtained from Gauss View program are shown in S1 for monomer and the dimer is shown in the supplementary data S2. The calculated bond lengths and bond angles for the optimized structures by B3LYP level using 6-311G(d,p) as basis set are presented in Table 1. To the best of our knowledge, experimental data on the geometric structure of the title compound are not available in the literature. The molecule 1PCA is composed of four peri-fused aromatic rings connected with the carboxylic acid group. The global minimum energy of 1PCA, calculated by DFT structure optimization method is −804.53530031 Hartree.

Interestingly the geometry optimization performed on the title compound indicated that it exhibits intramolecular hydrogen bond interaction. The intramolecular H-bond is preserved; the distance C17—H18···O28 of 2.079 Å and C1—H21···O27 of 2.315 Å are calculated the strong and weak interactions respectively using DFT method. The distance is slightly significantly shorter than that of the Van der Waals separation between the O atom and the H atom (2.72 Å) [22] indicating the existence of the C—H···O interaction in 1PCA. The exception of that hydrogen bonding influenced C—H bond lengths; apart from that the remaining bonds are almost same values ∼1.85 Å in the pyrene ring system. Particularly, the fused C4—C5 bond length value adopted maximum at 1.437 Å compare to the remaining bond lengths in that same case such as C8—C9 (1.427 Å), C8—C15 (1.423 Å), C3—C4 (1.427 Å) and C4—C8 (1.429 Å) respectively. The COOH substituted C6—C26 (1.494 Å) bond length having more pronounced single bond character.

The outer C—C—C angles having increased bond angles in which C6—C5—C17 (124.7°) is get the maximum value according to the hydrogen bonding between the neighboring hydrogen and oxygen atoms the remaining three are adopted the same value at ∼121° for their bond angles. Due to the weak interaction with C=O, the C6—C1—H21 bond angles contracted more at 117.4° while the remaining are keep this above 118° for the entire molecule. All the dihedral values strongly agreed the entire molecule should be in planar.

Vibrational analysis

The computational study was extended to vibrational spectroscopy for frequency as well as IR intensity and Raman activity analysis in order to support the assignment of experimental values of the vibration bands for 1PCA. The vibrational analysis was performed by frequency calculations of the optimized structure. The molecule consists of 29 atoms and has 81 normal modes of vibrations. These normal modes are distributed as 55 in-plane vibrations and 26 out-of-plane vibrations. The experimental and calculated wavenumbers along with their relative intensities, probable assignments and TED of 1PCA are summarized in Table 2. The calculated at B3LYP with the experimental reveals the overestimation of the calculated vibrational modes due to neglect of anharmonicity in real system. In order to improve the agreement with the experiment, the calculated wavenumbers are scaled with proper scaling factor. After applying a uniform scaling factor, the theoretical calculation reproduces the experimental data well. However, there are significant differences which can be attributed to the intermolecular hydrogen bonding.

C—H vibrations

The C—H stretching vibrations of aromatic and heteroaromatic structures generally occur in the region 3100–3000 cm^{-1} [23]. This permits the ready identifications of the structure. In the present work, the bands observed at 3041 and 2962 cm^{-1} in FT-IR spectrum are assigned to C—H stretching vibrations. Scaled vibrations assigned to the aromatic C—H stretching computed in the range 3129–3027 cm^{-1} for monomer and in the range 3128–3027 for dimer by B3LYP/6-311G(d,p) method along with the TED contribution of above 96% shows good agreement with the recorded FTIR spectral data. As evident from Table 2, the C—H stretching vibrations are pure stretching vibrations. The C—H in-plane-bending vibrations in aromatic compounds characterized by several medium to strong intensity bands in the region between 1300 and 1000 cm^{-1}. The C—H out-of-plane bending vibrations give rise to intense bands in the region between 1000 and 650 cm^{-1} [24]. When there is in-plane interaction above 1200 cm^{-1}, a carbon and its hydrogen usually move in opposite direction [24]. In this case, the C—H in-plane – bending vibrations are observed at 1264, 1181, 1151 and 1140 cm^{-1} in FTIR spectrum. The same vibrations are predicted at 1253, 1190, 1184, 1172 and 1150 cm^{-1} for monomer by B3LYP method. The C—H in-plane bending vibrations have substantial overlapping with the ring C—C stretching vibrations. The C—H out-of-plane deformation modes have established their peaks at 917, 869, 837 and 743 cm^{-1} in FTIR spectrum. The calculated out-of-plane mode

Table 1
Calculated optimized parameter values of the 1PCA [Bond length in (Å), angles in (°)].

Bond length	B3LYP	Bond angle	B3LYP	Dihedral angle	B3LYP
C1—C2	1.380	C2—C1—C6	122.1	C6—C1—C2—C3	0
C1—C6	1.403	C2—C1—H21	120.5	C6—C1—C2—H22	180
C1—21	1.082	C6—C1—H21	117.4	H21—C1—C2—C3	180
C2—C3	1.401	C1—C2—C3	120.5	H21—C1—C2—H22	0
C2—22	1.084	C1—C2—H22	120.1	C2—C1—C6—C5	0
C3—C4	1.427	C3—C2—H22	119.4	C2—C1—C6—C26	180
C3—C7	1.434	C2—C3—C4	119.1	H21—C1—C6—C5	180
C4—C5	1.437	C2—C3—C7	121.4	H21—C1—C6—C26	0
C4—C8	1.429	C4—C3—C7	119.5	C1—C2—C3—C4	0
C5—C6	1.423	C3—C4—C5	120.7	C1—C2—C3—C7	180
C5—C17	1.440	C3—C4—C8	118.8	H22—C2—C3—C4	180
C6—C26	1.494	C5—C4—C8	120.6	H22—C2—C3—C7	0
C7—C10	1.357	C4—C5—C6	118.1	C2—C3—C4—C5	0
C7—H20	1.085	C4—C5—C17	117.2	C2—C3—C4—C8	180
C8—C9	1.427	C6—C5—C17	124.7	C7—C3—C4—C5	180
C8—C15	1.423	C1—C6—C5	119.6	C7—C3—C4—C8	0
C9—C10	1.433	C1—C6—C26	113.1	C2—C3—C7—C10	180
C9—C11	1.402	C5—C6—C26	127.3	C2—C3—C7—H20	0
C10—H23	1.085	C3—C7—C10	121.3	C4—C3—C7—C10	0
C11—H12	1.085	C3—C7—H20	118.1	C4—C3—C7—H20	180
C11—C13	1.391	C10—C7—H20	120.5	C3—C4—C5—C6	0
C13—C14	1.390	C4—C8—C9	120.5	C3—C4—C5—C17	180
C13—H24	1.084	C4—C8—C15	120.3	C8—C4—C5—C6	180
C14—C15	1.403	C9—C8—C15	119.2	C8—C4—C5—C17	0
C14—H25	1.085	C8—C9—C10	118.8	C3—C4—C8—C9	0
C15—C16	1.430	C8—C9—C11	119.3	C3—C4—C8—C15	180
C16—C17	1.359	C10—C9—C11	121.8	C5—C4—C8—C9	180
C16—H19	1.085	C7—C10—C9	121.0	C5—C4—C8—C15	0
C17—H18	1.077	C7—C10—H23	120.5	C4—C5—C6—C1	0
H18—O28	2.079	C9—C10—H23	118.5	C4—C5—C6—C26	180
C26—O27	1.211	*Dihedral angle*	*B3LYP*	C17—C5—C6—C1	180
C26—O28	1.358	C8—C9—C11—H12	180	C17—C5—C6—C26	0
O28—H29	0.969	C8—C9—C11—C13	0	C4—C5—C17—C16	0
Bond angle	*B3LYP*	C10—C9—C11—H12	0	C4—C5—C17—H18	180
C11—C13—C14	120.3	C10—C9—C11—C13	180	C6—C5—C17—C16	180
C11—C13—H24	119.8	C9—C11—C13—C14	0	C6—C5—C17—H18	0
C14—C13—H24	119.9	C9—C11—C13—H24	180	C1—C6—C26—O27	0
C13—C14—C15	120.8	H12—C11—C13—C14	180	C1—C6—C26—O28	180
C13—C14—H25	120.2	H12—C11—C13—H24	0	C5—C6—C26—O27	180
C15—C14—H25	119.1	C11—C13—C14—C15	0	C5—C6—C26—O28	0
C8—C15—C14	119.6	C11—C13—C14—H25	180	C3—C7—C10—C9	0
C8—C15—C16	118.0	H24—C13—C14—C15	180	C3—C7—C10—H23	180
C14—C15—C16	122.4	H24—C13—C14—H25	0	H20—C7—C10—C9	180
C15—C16—C17	122.1	C13—C14—C15—C8	0	H20—C7—C10—H23	0
C15—C16—H19	118.4	C13—C14—C15—C16	180	C4—C8—C9—C10	0
C17—C16—H19	119.6	H25—C14—C15—C8	180	C4—C8—C9—C11	180
C5—C17—C16	121.9	H25—C14—C15—C16	0	C15—C8—C9—C10	180
C5—C17—H18	118.8	C8—C15—C16—C17	0	C15—C8—C9—C11	0
C16—C17—H18	119.4	C8—C15—C16—H19	180	C4—C8—C15—C14	180
C6—C26—O27	123.7	C14—C15—C16—C17	180	C4—C8—C15—C16	0
C6—C26—O28	116.3	C14—C15—C16—H19	0	C9—C8—C15—C14	0
O27—C26—O28	120.0	C15—C16—C17—C5	0	C9—C8—C15—C16	180
C26—O28—H29	105.2	C15—C16—C17—H18	180	C8—C9—C10—C7	0
C9—C11—H12	119.0	H19—C16—C17—C5	180	C8—C9—C10—H23	180
C9—C11—C13	120.9	H19—C16—C17—H18	0	C11—C9—C10—C7	180
H12—C11—C13	120.1	C6—C26—O28—H29	180	O27—C26—O28—H29	0

vibrations are found to be in good agreement with the observed values.

COOH vibrations

The carboxylic acid dimer is formed by strong hydrogen bonding interaction in the solid state. The intermolecular hydrogen bonding between 1PCA molecules can significantly affect the IR spectra. The carboxylic acid O—H stretching bands are weak in the Raman spectrum, so IR data are generally used. The O—H stretching is characterized by a broad band appearing near about 3400 cm^{-1} [25,26]. When the O—H in carboxylic acid do not form intramolecular bond, the stretching mode is to be expected at 3520 cm^{-1} [27,28]. In this study, the O—H stretching mode is calculated and assigned at 3597 cm^{-1} for carboxylic acid group. The O—H stretching vibration is observed at 3467 cm^{-1} for monomer and the deviation is due to the intermolecular hydrogen bonding. The O—H out-of-plane bending vibrations in dimer conformations are increased in value because of the hydrogen-bonding effect through the carboxyl groups. The calculated value of O—H out-of-plane bending vibration is 612 cm^{-1} for monomer, which is less than the dimer value of 988, 938 cm^{-1} and is in good agreement with the measured value of 596 cm^{-1}. The C=O stretching of carboxylic group is observed in FTIR spectrum at 1677 cm^{-1} and computed at 1693 cm^{-1} for monomer and 1647 cm^{-1} for dimer. The TED value of this mode is 82%.

C—C vibrations

The aromatic ring vibrational modes of title compound have been analyzed based on the vibrational spectra of previously published vibrations of the benzene molecule are helpful in the iden-

Table 2
Comparison of the experimental and calculated vibrational spectra and proposed assignments of 1PCA.

	Experimental	B3LYP/6-311G(d,p) //Monomer					B3LYP/6-311G(d,p) //Dimer		Assignments and (TED, ⩾10%)
	FT-IR	Unscaled	Scaled	I_{IR}[a]	SA_{Ra}[b]	I_{Ra}[c]	Unscaled	Scaled	Assignments
1		31	30	1.11	0.54	0.01	65, 14	64, 14	t COOH (89)
2		59	58	0.01	2.74	0.01	89, 57	87, 56	Butterfly (60)
3		107	105	0.23	0.05	0.00	115, 107	113, 105	γ CCCC (40)
4		178	175	0.40	0.10	0.00	184, 179	181, 176	γ CCCC (54)
5		202	198	0.14	1.19	0.00	242, 227	238, 223	r COOH (63)
6		213	210	8.90	0.30	0.00	212, 212	208, 208	γ CCCC (59)
7		267	262	0.15	0.46	0.00	266, 266	261, 261	γ CCCC (49)
8		284	279	0.08	0.19	0.00	291, 286	286, 281	γ CCCC (42)
9		315	309	0.29	7.01	0.41	344, 317	338, 312	β CCC (32) + υ C–COOH (20) + r COOH (19)
10		340	334	4.48	19.96	1.00	388, 372	381, 366	r COOH (36) + β CCC (19) + υ CC (13)
11		409	402	0.99	0.27	0.01	411, 410	404, 403	γ CCCC (48)
12		422	415	2.36	24.34	0.76	429, 424	422, 417	β CCC (48) + υ CC (11)
13		455	447	4.03	3.63	0.10	470, 460	462, 452	β CCC (46) + r COOH (17)
14	464	492	483	0.98	5.64	0.13	498, 495	490, 487	β CCC (32) + υ CC (13)
15	490	501	492	6.44	1.02	0.02	503, 502	494, 493	γ CCCC (47)
16		514	505	2.28	5.52	0.11	515, 514	506, 505	γ CCCC (56)
17	511	521	513	2.48	1.00	0.02	523, 522	514, 513	β CCC (49) + υ CC (13)
18	535	544	534	7.93	1.27	0.02	548, 547	539, 538	γ CCCC (33)
19		568	558	15.93	2.72	0.04	576, 571	566, 561	β CCC (37) + β OCO (13)
20	565	574	564	21.28	3.82	0.06	587, 586	577, 576	γ CCCC (28) + γ OH (25)
21		580	570	7.99	16.17	0.25	598, 593	588, 583	Ring breathing (42) + β OCO (12)
22	596	622	612	40.87	8.03	0.11	1005, 954	988, 938	γ OH (59)
23	630	636	625	10.53	22.98	0.29	645, 645	634, 634	υ CC (29) + β OCO (23)
24		691	679	0.15	0.11	0.00	690, 689	678, 677	γ CCCC (31)
25		707	695	0.34	0.10	0.00	708, 707	696, 695	Ring deformation (48)
26		711	699	49.17	1.75	0.02	754, 742	741, 729	β OCO (35) + υ CO (14)
27	706	725	713	52.67	0.13	0.00	721, 721	709, 709	γ CCCC (30) + γ CH (17)
28	743	766	753	26.81	0.07	0.00	765, 764	752, 751	γ CH (55) + γ CCCO (13)
29		780	767	6.17	1.28	0.01	792, 787	779, 774	Ring deformation (61)
30	777	782	768	5.95	0.13	0.00	778, 778	765, 765	γ CCCO (44) + γ CH (19)
31		818	804	1.32	1.68	0.01	819, 818	805, 804	γ CH (68)
32		828	814	8.46	2.33	0.02	826, 825	812, 811	γ CCCC (45) + γ CH (16)
33	820	834	819	6.27	0.33	0.00	833, 833	819, 819	β CCC (63) + υ CC (17)
34	837	854	840	34.38	0.17	0.00	855, 854	840, 839	γ CH (45) + γ CCCC (10)
35	847	871	857	5.57	1.42	0.01	884, 881	869, 866	Ring deformation (69)
36	869	874	860	59.02	0.48	0.00	874, 873	859, 858	γ CH (73)
37	917	916	901	0.17	1.04	0.01	918, 917	902, 901	γ CH (82)
38		980	963	0.29	0.04	0.00	981, 980	964, 963	γ CH (83)
39		987	971	0.03	0.13	0.00	988, 987	971, 970	γ CH (60)
40	974	990	973	0.65	1.25	0.01	991, 991	974, 974	υ CC (54) + β CCC (10)
41		997	980	0.04	1.68	0.01	997, 996	980, 979	γ CH (84)
42		1003	986	0.51	1.39	0.01	1000, 999	983, 982	γ CH (83)
43	1042	1056	1038	8.73	9.93	0.04	1065, 1064	1047, 1046	υ CC (29) + β CCC (13) + υ CO (10)
44	1091	1105	1086	53.30	9.86	0.03	1113, 1112	1094, 1093	υ CC (36) + β CH (24) + υ CO (13)
45		1131	1111	59.34	20.60	0.07	1132, 1132	1113, 1113	υ CC (28) + β CH (20)
46		1136	1116	131.28	9.56	0.03	1168, 1167	1148, 1147	υ CO (19) + υ CC (18)
47	1140	1170	1150	10.36	13.59	0.04	1178, 1177	1158, 1157	β CH (55) + υ CC (16)
48	1151	1192	1172	1.26	1.19	0.00	1191, 1190	1171, 1170	β CH (45) + υ CC (19)
49	1181	1204	1184	5.54	13.35	0.04	1205, 1205	1185, 1185	β CH (53) + υ CC (13)
50		1210	1190	134.35	101.07	0.27	1506, 1477	1480, 1452	β CH (30) + β OH (24) + υ CC (22)
51	1200	1223	1202	106.74	189.27	0.50	1223, 1222	1202, 1201	υ CC (39) + β CH (28)
52		1248	1226	31.30	274.72	0.68	1247, 1246	1226, 1225	υ CC (32) + β CH (22)
53	1234	1263	1241	4.72	277.29	0.67	1262, 1262	1241, 1241	υ CC (39) + β CH (38)
54	1264	1274	1253	3.84	22.67	0.05	1274, 1274	1252, 1252	β CH (42) + υ CC (24)
55		1326	1304	25.69	36.24	0.08	1310, 1307	1288, 1285	υ CC (23) + β OH (18) + β CH (13)
56	1326	1340	1317	7.22	10.08	0.02	1341, 1340	1318, 1317	υ CC (57) + β CH (13)
57		1383	1359	79.51	29.55	0.06	1358, 1356	1335, 1333	υ CC (22) + β OH (18) + υ CO (14)
58		1392	1369	1.47	41.80	0.08	1393, 1393	1369, 1369	υ CC (69)
59	1384	1401	1377	18.97	108.55	0.20	1401, 1401	1377, 1377	υ CC (63)
60	1400	1433	1408	6.21	92.75	0.16	1432, 1431	1408, 1407	υ CC (38) + β CH (25)
61	1420	1442	1418	1.89	47.05	0.08	1443, 1442	1418, 1417	β CH (63) + υ CC (12)
62	1436	1465	1440	3.49	10.49	0.02	1461, 1455	1436, 1430	β CH (31) + υ CC (22)
63	1458	1488	1463	3.22	3.78	0.01	1488, 1486	1463, 1461	υ CC (41) + β CH (31)
64		1516	1491	9.39	39.24	0.06	1518, 1518	1492, 1492	υ CC (52) + β CH (21)
65	1508	1540	1514	32.22	33.44	0.05	1543, 1541	1517, 1515	υ CC (33) + β CH (13)
66	1542	1576	1549	0.86	34.91	0.05	1577, 1576	1550, 1549	υ CC (63)
67	1584	1620	1592	3.17	185.50	0.23	1621, 1621	1593, 1593	υ CC (62)
68	1596	1629	1601	54.85	348.37	0.42	1631, 1631	1603, 1603	υ CC (64)
69	1625	1647	1619	32.19	61.28	0.07	1649, 1648	1621, 1620	υ CC (65)
70		1666	1637	14.67	560.39	0.64	1667, 1667	1639, 1639	υ CC (60)
71	1677	1767	1693	491.53	222.19	0.21	1719, 1673	1647, 1647	υ C═O (82)
72	2962	3160	3027	0.89	24.50	0.00	3161, 3160	3028, 3027	υ CH (98)
73		3162	3029	1.63	31.77	0.00	3162, 3162	3029, 3029	υ CH (99)

(*continued on next page*)

Table 2 (*continued*)

	Experimental	B3LYP/6-311G(d,p) //Monomer					B3LYP/6-311G(d,p) //Dimer		Assignments and (TED, ⩾10%)
	FT-IR	Unscaled	Scaled	I_{IR}[a]	SA_{Ra}[b]	I_{Ra}[c]	Unscaled	Scaled	Assignments
74		3164	3031	6.09	108.44	0.02	3166, 3165	3033, 3032	υ CH (97)
75		3170	3037	20.69	159.53	0.02	3171, 3170	3038, 3037	υ CH (96)
76	3041	3172	3039	4.02	125.17	0.02	3172, 3172	3039, 3039	υ CH (97)
77		3179	3046	32.75	254.99	0.03	3180, 3180	3046, 3046	υ CH (98)
78		3187	3053	32.11	443.28	0.06	3187, 3187	3053, 3053	υ CH (99)
79		3210	3075	2.42	155.53	0.02	3216, 3214	3081, 3079	υ CH (100)
80		3266	3129	8.21	92.15	0.01	3269, 3265	3132, 3128	υ CH (99)
81	3467	3755	3597	106.57	233.65	0.02	3149, 3054	3017, 2926	υ OH (100)

ν: stretching, β: in-plane bending, γ: out-of-plane bending, t: twisting, r: rocking [frequency (cm^{-1}), [a]I_{IR} – IR Intensity (K $mmol^{-1}$), [b]SA_{Ra} – Raman scattering activities ($Å^4$ amu^{-1})], [c]I_{Ra} – Raman intensity (Arb units).

tification of the phenyl ring modes [29,30]. The ring stretching vibrations are very much important in the spectrum of benzene and its derivatives, and are highly characteristics of the aromatic ring itself. The aromatic ring carbon–carbon stretching vibrations occur in the region 1430–1625 cm^{-1}. In the present investigation, the C—C aromatic stretch is observed in the region 1625–1326 cm^{-1} in the FTIR spectrum. These vibrational wavenumbers are in agreement with the calculated wavenumbers in the range 1637–1317 cm^{-1} by DFT method. The ring out-of-plane bending vibrations are observed at low wavenumber region. The butterfly mode is calculated at 58 cm^{-1} for monomer and at 87, 56 cm^{-1} for dimer. The predicted values of both monomer and dimer molecules well reproduce the experimental data.

Absorption spectra

On the basis of the fully optimized ground-state structure, TD-DFT/B3LYP/6-311G(d,p) calculations have been performed to determine the low-lying excited states of 1PCA. The calculated result involving the vertical excitation energies, oscillation strength (*f*) and wavelength were carried out and compared with the measured experimental wavelength listed in Table 3. Calculations are performed for gas phase and ethanol, methanol, water and DMSO environment. The TD-DFT method is able to detect accurate absorption wavelengths at a relatively small computing time which correspond to vertical electronic transitions computed on the ground state geometry, especially in the study of solvent effect for vertical excitation energy of electronic spectra [31–33]. Typically, according to the Frank–Condon principle, the maximum absorption peak λ_{max} corresponds in an UV–Vis spectrum to vertical excitation. TD-DFT/B3LYP/6-311G(d,p) method predicts two intense electronic transition at 3.3001 eV (375.70 nm) and 4.3781 eV

Table 3
The experimental and computed absorption wavelength λ (nm), excitation energies *E* (eV), absorbance and oscillator strengths (*f*) of 1PCA in ethanol solution (top) and gas phase and another different solvents (bottom).

Experimental (in ethanol)			TD-B3LYP/6-31G(d,p) (in ethanol)		
E (eV)	λ (nm)	Abs.	*E* (eV)	λ (nm)	*f*
3.3023	375.5	0.010	3.3001 (64 → 65)	375.70	0.4695
3.6099	343.5	0.294	3.6316 (63 → 65)	341.40	0.0320
3.7747	328.5	0.212	4.1750 (62 → 65)	296.97	0.0250
4.4846	276.5	0.298	4.3781 (64 → 66)	283.19	0.2556
4.6529	266.5	0.145	4.4737 (64 → 67)	277.14	0.0559
5.0924	243.5	0.441	4.6110 (60 → 65)	268.89	0.0001
5.2878	234.5	0.275	4.7500 (64 → 68)	261.02	0.0024
E (eV)	λ (nm)	*f*	*E* (eV)	λ (nm)	*f*
Gas			*Methanol*		
3.3888 (64 → 65)	365.86	0.3365	3.3047 (64 → 65)	375.17	0.4594
3.6356 (63 → 65)	341.03	0.0309	3.6323 (63 → 65)	341.34	0.0318
4.1979 (62 → 65)	295.35	0.0113	4.1754 (62 → 65)	296.94	0.0239
4.4305 (64 → 66)	279.84	0.1711	4.3812 (64 → 66)	282.99	0.2465
4.4833 (64 → 67)	276.55	0.0605	4.4746 (64 → 67)	277.08	0.0586
4.4926 (61 → 65)	275.98	0.0001	4.6126 (60 → 65)	268.80	0.0001
4.7590 (64 → 68)	260.53	0.0051	4.7503 (64 → 68)	261.00	0.0024
DMSO			*Water*		
3.2912 (64 → 65)	376.72	0.4861	3.3034 (64 → 65)	375.33	0.4607
3.6311 (63 → 65)	341.45	0.0322	3.6324 (63 → 65)	341.33	0.0318
4.1738 (62 → 65)	297.05	0.0276	4.1750 (62 → 65)	296.97	0.0243
4.3723 (64 → 66)	283.56	0.2675	4.3806 (64 → 66)	283.03	0.2462
4.4720 (64 → 67)	277.24	0.0538	4.4744 (64 → 67)	277.10	0.0596
4.6139 (60 → 65)	268.72	0.0001	4.6155 (60 → 65)	268.63	0.0001
4.7495 (64 → 68)	261.05	0.0023	4.7502 (64 → 68)	261.01	0.0023

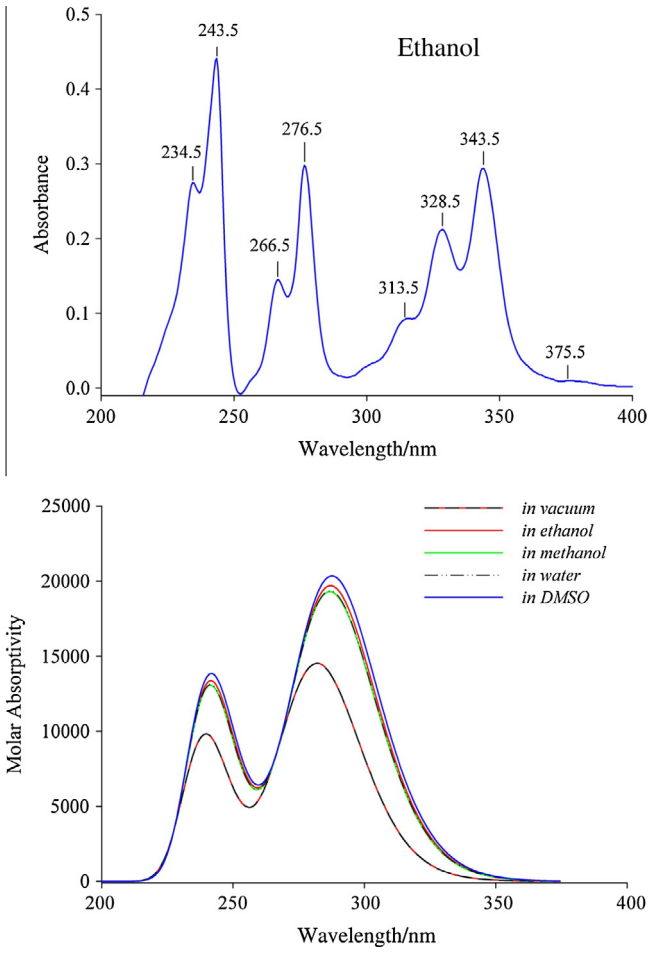

Fig. 3. Comparison of experimental (top) and theoretical in various solvents (bottom) UV–Vis spectrum of 1PCA.

(283.19 nm) with oscillator strength $f = 0.4695$ and 0.2556 respectively in good agreement with the measured experimental data in Ethanol solution (exp = 375.5 nm and 276.5 nm) as shown in Fig. 3. Other solvents are used to show the accuracy of our calculation with the experimental observation which is shown in Table 3. All the structures allowed strong π–π^* and σ–σ^* transition in the UV–Vis region with high extinction coefficients. The π–π^* transitions were expected to occur relatively at lower wavelengths, due to the consequence of the extended aromaticity of the benzene ring. Comparing these values with the corresponding experimental values, TD-DFT method for both in gas phase and solvent media is useful to predict UV–Vis spectrum. Molecular orbital coefficients analysis based on optimized geometry indicate that, for the title compound, the frontier molecular orbitals are mainly composed of π-atomic orbitals, so the electronic transitions are mainly derived from the contribution of bands $\pi \rightarrow \pi^*$ within the 1PCA molecule.

^1H and ^{13}C NMR analysis

Density functional theory shielding calculations are rapid and applicable to large systems, but the paramagnetic contribution to the shielding tends to be overestimated. In this sense, theoretical calculations of the chemical shifts may be used as an aid for the assignment of the experimental data and for the study of our title molecule. The calculated values of ^{13}C and ^1H chemical shifts by B3LYP/6-311++G(d,p) level of theory in the DMSO environment are summarized for both the monomer and dimer in Table 4. The observed ^1H and ^{13}C NMR spectra of the 1PCA molecule are given in Figs. 4 and 5, respectively. The experimental values are also included in Table 4. It is noted that the maximum deviation from experimental chemical shift for ^{13}C NMR chemical shift is 4.2 and 3.1 ppm (C6 atom) and the ^1H chemical shift, the maximum deviation from experimental value is 6.71 and 1.05 ppm (H29) for monomer and dimer respectively in DMSO solution. The cumulative influence of oxygen atoms (O27 and O28) in the 1PCA molecule reduces the electron density of the carbon atom C26, thus its NMR signal is observed in the very downfield at 169.5 ppm. Due to the substitution of COOH group, the C6 NMR signal is observed in the shielding region at 123.9 ppm with maximum deviation from the calculated values both monomer and dimer. In the pyrene ring system, the only atoms C3, C5, C9 and C15 having downfield NMR signal at 134, 131.1, 130.6 and 130.3 ppm. While, due to the more electron density of all the carbon atoms, their NMR signal is observed in the shielding region at the range of 123.9–134 ppm.

Owing to the intra molecular interaction H18 and H21 proton NMR chemical shifts are appear in the deshielding region at 9.25 and 8.62 ppm respectively. In that case, the strong and weak interaction dominates the values of chemical shift. Due to the electron withdrawing environmental, the H29 chemical shifts are observed in the deshielded region at maximum of 13.34 ppm appear as singlet peak. There is no maximum impact in the electron density of peri-fused pyrene ring, so that the remaining hydrogens are appear in multiplet peaks. Owing to this fact, all the remaining protons are overlapped and appear as multiplet peak in the ^1H NMR spectrum with shielded values are measured between the range of 8.14–8.39 ppm. The calculated and experimental chemical shift values are given in Table 4 shows a good agreement with each other and also the gas phase.

HOMO LUMO analysis

In order understanding the bonding feature of the title molecule, plot of the Frontier orbitals, the second highest and highest occupied molecular orbitals are very important HOMO and HOMO−1 and second highest and lowest unoccupied molecular orbitals LUMO and LUMO+1 as shown in Fig. 6. The conjugated molecules are characterized by a highest occupied molecular orbital-lowest unoccupied molecular orbital (HOMO–LUMO) separation, which is the result of a significant degree of intermolecular charge transfer (ICT) from the end-capping electron-donor to the efficient electron acceptor group through p-conjugated path. The HOMO is the orbital that primarily acts as an electron donor and the LUMO is the orbital that largely acts as the electron acceptor, and the gap between HOMO and LUMO characterizes the molecular chemical stability. The energy gap between the HOMO and the LUMO molecular orbitals is a critical parameter in determining molecular electrical transport properties because it is a measure of electron conductivity. The highest occupied molecular orbitals are localized mainly on the pyrene ring system. On the other hand, the lowest unoccupied molecular orbitals are localized over the entire molecule. The computed energy values of HOMO and LUMO in gas phase are −5.8573 eV and −2.3182 eV, respectively. The energy gap value is 3.5391 eV for 1PCA molecule. The energy values of the frontier orbitals of different solution are presented in Supplementary data S3. The energy gap between HOMO and LUMO determines the kinetic

Table 4
The observed (in DMSO) and predicted ^1H and ^{13}C NMR isotropic chemical shifts (with respect to TMS, all values in ppm) for 1PCA monomer and dimer.

Atom	Exp.	B3LYP/6-311++G(d,p)				Atom	Exp.	B3LYP/6-311++G(d,p)			
	DMSO	Monomer		Dimer			DMSO	Monomer		Dimer	
		Gas	DMSO	Gas	DMSO			Gas	DMSO	Gas	DMSO
H12	8.39	8.16	8.51	8.16	8.54	C4	125.0	125.0	125.3	124.6	124.8
H18	9.25	9.67	9.79	10.02	10.04	C5	131.1	132.8	133.4	134.0	134.3
H19	8.36	8.13	8.47	8.27	8.59	C6	123.9	120.0	119.7	121.2	120.8
H20	8.24	7.95	8.27	7.98	8.31	C7	127.1	127.4	128.4	127.2	128.2
H21	8.62	9.24	9.25	9.42	9.49	C8	124.5	124.2	124.2	124.5	124.6
H22	8.31	8.06	8.36	8.12	8.44	C9	130.6	131.4	131.8	130.7	131.1
H23	8.33	8.08	8.44	8.08	8.45	C10	129.6	130.7	132.6	130.6	132.6
H24	8.14	8.00	8.33	8.05	8.38	C11	126.6	126.2	128.4	126.2	128.5
H25	8.39	8.16	8.53	8.27	8.61	C13	125.1	125.5	127.3	125.1	127.0
H29	13.34	5.92	6.63	14.37	14.39	C14	126.9	126.3	128.2	126.5	128.3
Atom						C15	130.3	130.4	130.5	130.1	130.2
C1	129.9	133.1	133.0	132.4	132.7	C16	128.9	129.8	131.7	130.0	131.7
C2	124.9	123.2	124.3	122.8	124.1	C17	127.6	127.2	127.0	127.2	126.5
C3	134.0	136.0	137.0	136.3	137.3	C26	169.5	166.5	168.8	175.3	176.3

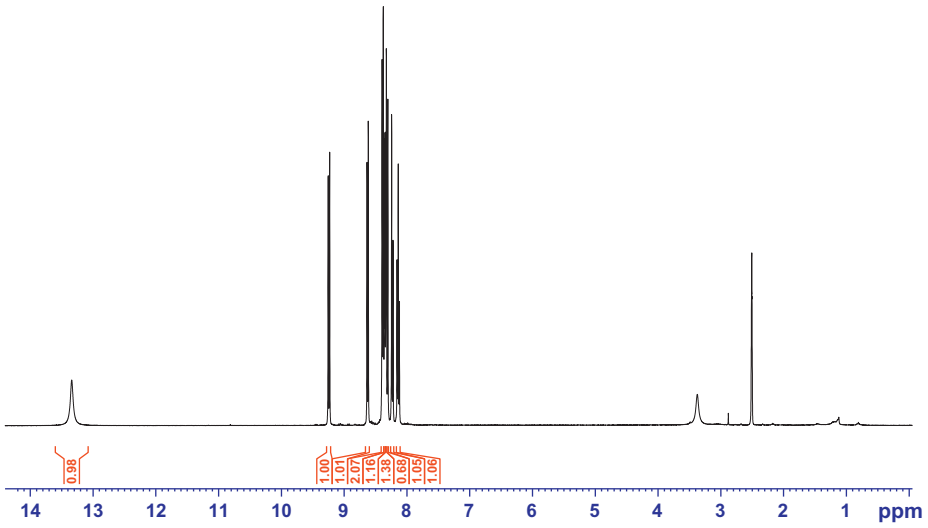

Fig. 4. ^{1}H NMR spectrum of 1PCA.

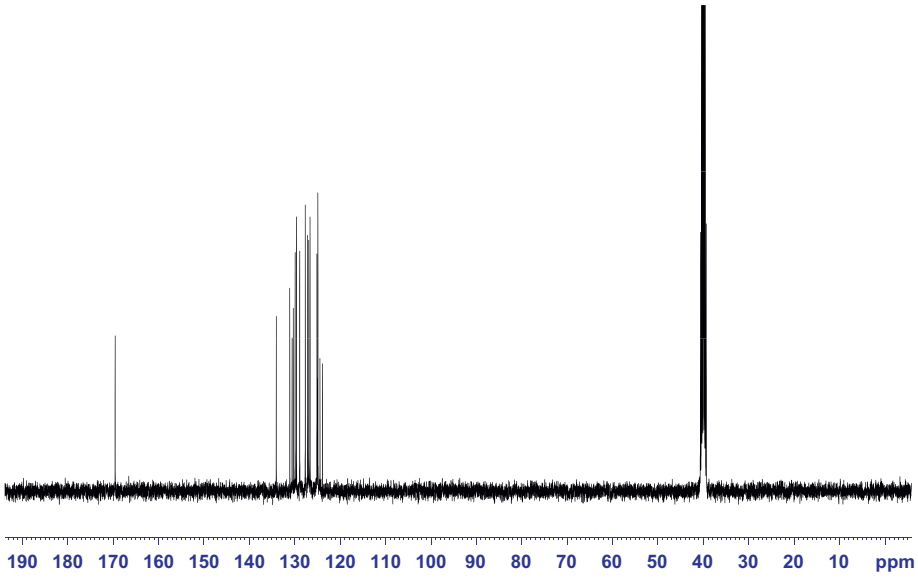

Fig. 5. ^{13}C NMR spectrum of 1PCA.

stability, chemical reactivity and, optical polarizability and chemical hardness–softness of a molecule [34].

Molecular electrostatic potential (MEP)

In order to predict the molecular reactive sites, the MEP for our title molecule is calculated by B3LYP/6-311G(d,p) method as shown in Fig. 7. Molecular electrostatic potential (MEP) generally present in the space around the molecule by the charge distribution is very useful in understanding the sites of electrophilic attacks and nucleopilic reaction for the study of biological recognition process [35] and hydrogen bonding interactions [36]. The different values of the electrostatic potential at the surface are represented by different colors. Potential increases in the order red < orange < yellow < green < blue. The color code of these maps is in the range between −33.6343 a.u (deepest red) and 33.6343 a.u (deepest blue) in compound, where blue indicates the strongest attraction and red indicates the strongest repulsion. As can be seen from the MEP map of the title molecule, while regions having the negative potential are over the electronegative atom (oxygen atoms), the regions having the positive potential are over the hydrogen atoms. From these results, we can say that the H atoms indicate the strongest attraction and O atom indicates the strongest repulsion.

Nonlinear optical effects

Nonlinear optical (NLO) effects arise from the interactions of electromagnetic fields in various media to produce new fields altered in phase, frequency, amplitude or other propagation characteristics from the incident fields [37]. The first hyperpolarizability (β_0) of this novel molecular system, and related properties (β, α_0 and $\Delta\alpha$) of 1PCA are calculated using HF/6-311G(d,p) method, based on the finite-field approach. In the presence of an applied electric field, the energy of a system is a function of the electric field. First order hyperpolarizability is a third rank tensor that can be described by $3 \times 3 \times 3$ matrices. The 27 components of the 3D matrix can be reduced to 10 components due to the

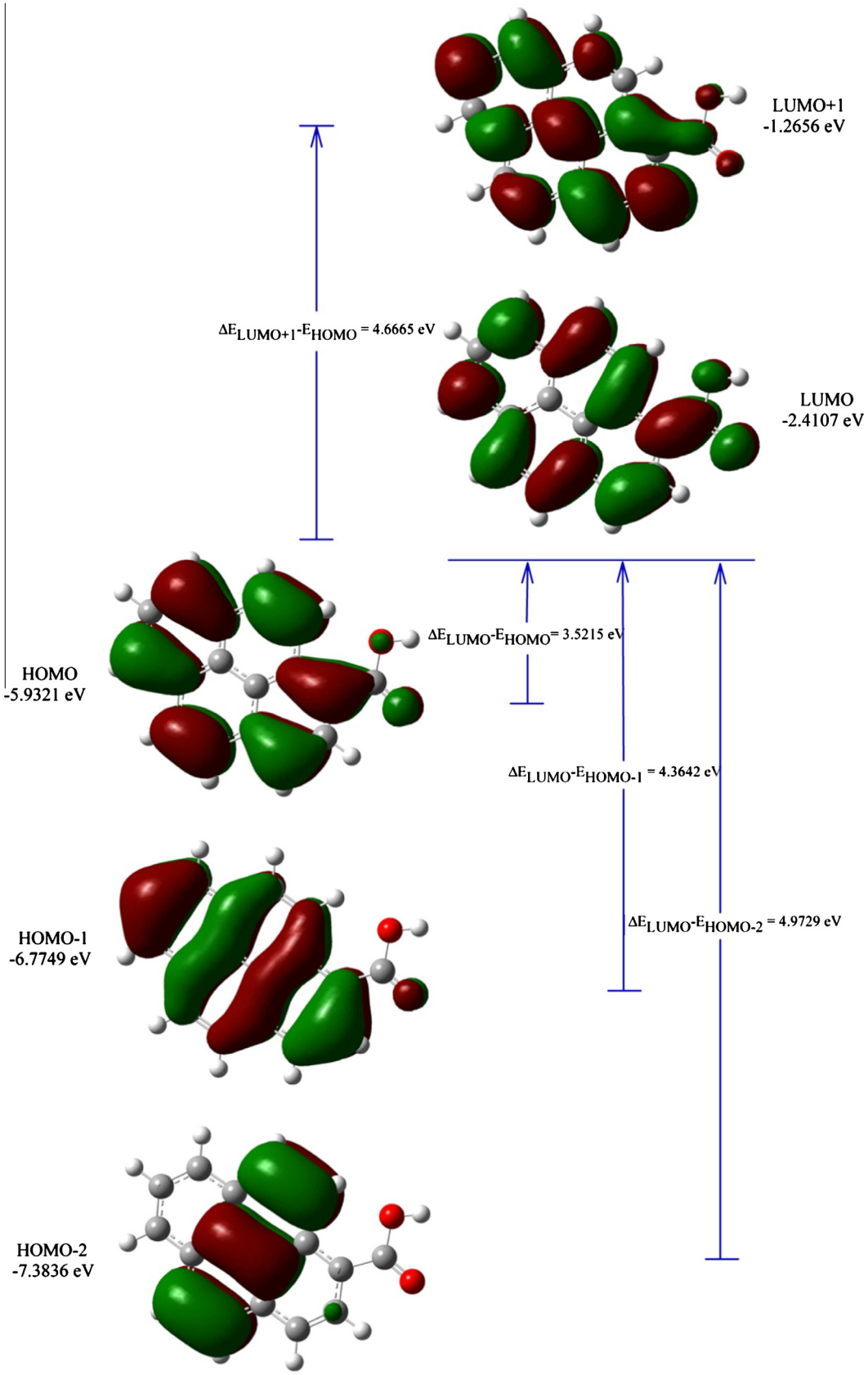

Fig. 6. The atomic orbital compositions of the frontier molecular orbital for 1PCA.

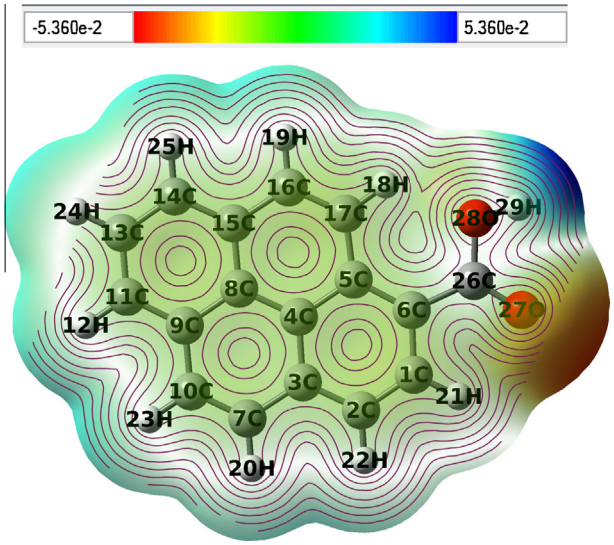

Fig. 7. Molecular electrostatic potential map of 1PCA calculated by B3LYP/6-311G(d,p) method.

Kleinman symmetry [38]. It can be given in the lower tetrahedral format. It is obvious that the lower part of the $3 \times 3 \times 3$ matrices is a tetrahedral. The components of β are defined as the coefficients in the Taylor series expansion of the energy in the external electric field. When the external electric field is weak and homogeneous, this expansion becomes:

$$E = E^0 - \mu_\alpha F_\alpha - 1/2\alpha_{\alpha\beta}F_\alpha F_\beta - 1/6\beta_{\alpha\beta\gamma}F_\alpha F_\beta F_\gamma + \cdots$$

where E^0 is the energy of the unperturbed molecules, F_α is the field at the origin, μ_α, $\alpha_{\alpha\beta}$ and $\beta_{\alpha\beta\gamma}$ are the components of dipole moment, polarizability and the first order hyperpolarizabilities, respectively. The total static dipole moment μ, the mean polarizability α_0, the anisotropy of the polarizability Δ_α and the mean first order hyperpolarizability β_0, using the x, y, z components they are defined as:

$$\mu = \left(\mu_x^2 + \mu_y^2 + \mu_z^2\right)^{1/2}$$

$$\alpha_0 = (\alpha_{xx} + \alpha_{yy} + \alpha_{zz})/3$$

$$\alpha = 2^{-1/2}[(\alpha_{xx} - \alpha_{yy})^2 + (\alpha_{yy} - \alpha_{zz})^2 + (\alpha_{zz} - \alpha_{xx})^2 + 6\alpha^2 xx]^{1/2}$$

$$\beta_0 = (\beta_x^2 + \beta_y^2 + \beta_z^2)^{1/2}$$

and

$$\beta_x = \beta_{xxx} + \beta_{xyy} + \beta_{xzz}$$

$$\beta_y = \beta_{yyy} + \beta_{xxy} + \beta_{yzz}$$

$$\beta_z = \beta_{zzz} + \beta_{xxz} + \beta_{yyz}$$

Since the values of the polarizabilities (α) and hyperpolarizability (β) of the Gaussian 03 output are reported in atomic units (a.u.), the calculated values have been converted into electrostatic units (esu) (α: 1 a.u. = 0.1482×10^{-24} esu; β: 1 a.u. = 8.639×10^{-33} esu). The total molecular dipole moment and first order hyperpolarizability are 2.6193 Debye and 7.634×10^{-30} esu, respectively and are depicted in Table 5. Total dipole moment of title molecule is approximately two times greater than that of urea and first order hyperpolarizability is 20 times greater than that of urea (μ and β of urea are 1.3732 Debye and 0.3728×10^{-30} esu obtained by HF/6-311G(d,p) method). This result indicates the nonlinearity of the 1PCA molecule.

Table 5
The polarizability and first order hyperpolarizability of 1PCA.

	a.u.	esu ($\times 10^{-24}$)		a.u.	esu ($\times 10^{-30}$)
α_{xx}	326.441305	48.379	β_{xxx}	−435.0636353	−3.759
α_{xy}	18.0587736	2.676	β_{xxy}	−370.1553379	−3.198
α_{yy}	225.2372084	33.380	β_{xyy}	−309.6195623	−2.675
α_{xz}	0	0.000	β_{yyy}	−138.7385058	−1.199
α_{yz}	0	0.000	β_{xxz}	0	0.000
α_{zz}	69.0364065	10.231	β_{xyz}	0	0.000
α_{tot}	206.9049733	30.663	β_{yyz}	0	0.000
$\Delta\alpha$	226.7762744	33.608	β_{xzz}	16.4558058	0.142
			β_{yzz}	8.3551896	0.072
			β_{zzz}	0	0.000
			β_{tot}	883.659481	7.634

Conclusion

The FTIR and FT-Raman spectra have been studied. The equilibrium geometries, harmonic wavenumbers and TD/DFT calculations of 1PCA molecule have been carried for the first time using DFT/B3LYP/6-311G(d,p) level of theory. Optimized geometrical parameters of the title compound have been calculated. The theoretically constructed FTIR and FT-Raman spectra have shown good correlation with experimentally observed FTIR and FT-Raman spectra. From the optimized geometry results, we can conclude that the 1PCA molecule is highly conjugated and π electron delocalized. The ^{1}H and ^{13}C NMR chemical shifts have been calculated and compared with the experimental one. The calculated dipole moment and first order hyperpolarizability results indicate that the title compound is a good candidate of NLO material. The UV spectrum was measured in ethanol solution. HUMO and LUMO orbitals have been visualized. The MEP map shows that the negative potential sites are on electronegative atoms while the positive potential sites are around the hydrogen atoms.

Appendix A. Supplementary material

Supplementary data associated with this article can be found, in the online version, at http://dx.doi.org/10.1016/j.saa.2013.05.086.

References

[1] S.M. Barlow, R. Raval, Surf. Sci. Rep. 50 (2003) 201–342.
[2] H. Idriss, M.A. Barteau, Adv. Catal. 45 (2000) 261–331.
[3] T. Higashi, T. Ichikawa, S. Inagaki, J.Z. Min, T. Fukushima, T. Toyo'oka, J. Pharm. Biomed. Anal. 52 (2010) 809–818.
[4] S.L. Murov, I. Carmichael, G.L. Hug, Handbook of Photochemistry, second ed., Marcel Dekker, New York, NY, 1993.
[5] S. Murata, R. Nakatsuji, H.J. Tomioka, J. Chem. Soc., Perkin Trans. 2 (1995) 793.
[6] S. Ikeda, S. Murata, K. Ishii, H. Hamaguchi, Bull. Chem. Soc. Jpn. 73 (2000) 2483–2590.
[7] M.J. Frisch, Gaussian 03, Revision B.01, Gaussian Inc., Pittsburgh, PA, 2003.
[8] S.F. Sousa, P.A. Fernandes, M.J.J. Ramos, Phys. Chem. A 111 (2007) 10439–10452.
[9] C.J. Cramer, D.G. Truhlar, Phys. Chem. Chem. Phys. 11 (2009) 10757–10816.
[10] R.Dennington II, T.Keith, J. Millam, Gauss View, Version 4.1.2, Semichem, Inc., Shawnee Mission, KS, 2007.
[11] M.H. Jamroz, Vibrational Energy Distribution Analysis, VEDA 4 Computer Program, Poland, 2004.
[12] E. Runge, E.K.U. Gross, Phys. Rev. Lett. 52 (1984) 997–1000.
[13] R.E. Stratmann, G.E. Scuseria, M.J. Frisch, J. Chem. Phys. 109 (1998) 8218–8224.
[14] R. Bauernschmitt, R. Ahirichs, Chem. Phys. Lett. 256 (1996) 454–464.
[15] M.E. Casida, C. Jamorski, K.C. Casida, D.R. Salahub, J. Chem. Phys. 108 (1998) 4439–4449.
[16] S. Miertuš, Chem. Phys. 55 (1981) 117–129.
[17] V. Barone, M. Cossi, J. Phys. Chem. 102A (1998) 1995–2001.
[18] M. Cossi, N. Rega, G. Scalmani, V. Barone, J. Comput. Chem. 24 (2003) 669–681.
[19] J. Tomasi, B. Mennucci, R. Cammi, Chem. Rev. 105 (2005) 2009–3093.
[20] G. Keresztury, S. Holly, G. Besenyei, J. Varga, A. Wang, J.R. Durig, Spectrochim. Acta 49A (1993) 2007–2017. 2019–2026.
[21] G. Keresztury, J.M. Chalmers, P.R. Griffith (Eds.), Raman Spectroscopy: Theory, Hand Book of Vibrational Spectroscopy, vol. 1, John Wiley & Sons Ltd., New York, 2002.

[22] H. Sato, J. Dybal, R. Murakami, I. Noda, Y. Ozaki, J. Mol. Struct. 744 (2005) 35–46.
[23] L.J. Bellamy, The Infrared Spectra of Complex Molecules, John Wiley, New York, 1956.
[24] J. Mohan, Organic Spectroscopy, Principle and Applications, second ed., New Age International (P) Limited Publishers, New Delhi, 2001.
[25] D. Lin-Vein, N.B. Colthup, W.G. Fataley, J.G. Grasselli, The Handbook of Infrared and Raman Characteristic Frequencies of Organic Molecules, Academic Press, San Diego, 1991.
[26] M. Silverstein, G. Clayton Basseler, C. Morill, Spectrometric Identification of Organic Compounds, Wiley, New York, 1981.
[27] D.A. Kleinman, J. Phys. Rev. 126 (1962) 1977–1979.
[28] C.A. Tellez, S.E. Hollauer, M.A. Mondragon, V.M. Castano, Spectrochim. Acta 57A (2001) 993–1007.
[29] G. Socrates, Infrared Characteristic Group Frequencies, Wiley Interscience Publication, 1980.
[30] G. Varsanyi, Vibrational Spectra of Benzene Derivatives, Academic Press, New York, 1969.
[31] D. Jacquemin, J. Preat, E.A. Perpete, Chem. Phys. Lett. 40 (2005) 254–259.
[32] D. Jacquemin, J. Preat, M. Charlot, V. Wathelet, J.M. Andre, E.A. Perpete, J. Chem. Phys. 121 (2004) 1736–1743.
[33] M. Cossi, V. Barone, J. Chem. Phys. 115 (2001) 4708–4717.
[34] B. Kosar, C. Albayrak, Spectrochim. Acta 78A (2011) 160–167.
[35] P. Politzer, P.R. Laurence, K. Jayasuriya, Olecular electrostatic potentials: an effective tool for the elucidation of biochemical phenomena, Environ. Health Perspect. 61 (1985) 191–202.
[36] P. Politzer, P. Lane, Molecular electrostatic potentials: concepts and applications, Struct. Chem. 61 (1990) 159–164.
[37] Y.X. Sun, Q.L. Hao, W.X. Wei, Z.X. Yu, L.D. Lu, X. Wang, Y.S. Wang, J. Mol. Struct. (Theochem) 904 (2009) 74.
[38] D.A. Kleinman, Phys. Rev. 126 (1962) 1977–1979.